Hindawi
Shock and Vibration
Volume 2020, Article ID 8875268, 19 pages
https://doi.org/10.1155/2020/8875268

Research Article

Design of a Tuned Mass Damper Inerter (TMDI) Based on an Exhaustive Search Optimization for Structural Control of Buildings under Seismic Excitations

Luis Augusto Lara-Valencia, Yosef Farbiarz-Farbiarz, and Yamile Valencia-González

Department of Civil Engineering, Universidad Nacional de Colombia, Medellín 050034, Colombia

Correspondence should be addressed to Luis Augusto Lara-Valencia; lualarava@unal.edu.co

Received 29 May 2020; Revised 10 July 2020; Accepted 6 August 2020; Published 25 August 2020

Academic Editor: Anindya Ghoshal

A tuned mass damper inerter (TMDI) is a new class of passive control device based on the inclusion of an inerter mechanism into a conventional tuned mass damper (TMD). The inerter device provides inertial resisting forces to the controlled system, through relatively small masses, converting it in a mechanism with the potential to enhance the performance of passive energy dissipating systems. This work presents a study of an optimal TMDI design through an exhaustive search process. TMDI device design using the cited parameter selection methodology consists in the determination of the damper critical damping ratio, ζ_{TMDI}, and frequency ratio, υ_{TMDI}, which result in the minimum structural response of a multidegree of freedom structural system, considering predefined values for mass ratio (μ) and inertance ratio (β). The used optimization process examines all possible damping device design parameter combinations to select the set of values that results in the best device performance to reduce response parameters in a structure. Four different optimization processes are performed by independently minimizing four performance indices: J_1 associated to the reduction of the structure's maximum peak displacement, J_2 calculates the minimal RMS value for the structure's peak displacement, J_3 seeks by the minimal peak interstorey drift, and J_P determines the lowest value for a linear weighted combination of the abovementioned three indices. A numerical example is developed with the purpose of validating the proposed optimization procedure and to evaluate the benefits of using TMDI as controlling devices for structures under seismic excitation, by carrying out a comparative analysis to contrast the performance of the optimization alternatives developed, running up to 1968192 cases. The obtained results show that devices designed based on exhaustive search optimization produce peak displacement reductions of up to 35% and peak structure displacement *RMS* reductions of up to 30%.

1. Introduction

Structural control is, fundamentally, a set of techniques that aims to reduce risks associated with the exposure of structures to random events originated in natural phenomena such as earthquakes, wind, and the effects of coastal waves. The main motivation for structural control is the possibility of providing with high level safety, comfort, and peace of mind to the people that inhabit the controlled structures. Structural control may be achieved through the use of diverse types of devices, mechanisms, and algorithms with varied levels of structural behavior. Successful structural control methodologies have been developed based on the modification of the structural system's stiffness, mass, shape, or damping [1], achieving noteworthy reductions in the structural response of systems subjected to the action of forces of diverse origins.

Current structural control applications are adjusted to diverse objectives and embody different variants, with devices and algorithms based on principles that may be grouped into four categories, according to the available literature: active control [2–4], passive control [5–10], semiactive control [11–15], and hybrid control [16–20]. Passive and active controlling devices represent the ends of the structural control theory spectrum; for active devices, their behavior results on the supply of large quantities of

energy to the structural system, while in passive devices, their behavior results in the use inertial forces within the structure achieving reduction in the structural response through energy dissipation mechanisms without the need for external power sources. Semiactive and hybrid devices correspond to intermediate solutions in which the working mechanisms use characteristics of both active and passive devices with low energy consumption.

Due to their simplicity, reliability, economy, and sturdiness, passive control devices stand out among structural control alternatives, especially the devices known as tuned mass dampers (TMDs). These mechanisms, composed by a mass, a spring, and a damper, are some of the oldest vibration control devices in existence [21]; moreover, their proved efficiency for the damage reduction and collapse prevention of structural systems [22], as they are tuned to the fundamental frequencies of the structure, make them ideal mechanisms to protect the structural integrity of a building. Some of the most representative applications of TMD can be found in base isolation [23–26], seismic protection of buildings [27–30], effect in soil-structure interaction [31–33], and vibration control of pedestrian bridges [34, 35], among others. According to their functioning mechanism, TMD are classified into conventional TMD, pendulum TMD (PTMD), bidirectional TMD (BTMD), and liquid column tuned dampers (TLCD) [36].

Searching for improvement in the performance of these devices, an important number of researchers have been working during the last five years with a promising modification of conventional TMD, consisting in the addition of a two-node linear device, called an inerter, that develops an internal resisting force proportional to the relative acceleration between the two nodes [37]. This new device composed by an inerter and a conventional TMD has been called the tuned mass damper inerter (TMDI). Several research works have explored the design [38–40], optimization [39–42], and performance [43–45] of this new passive control device with positive results, proving that these mechanisms may outperform the conventional TMD output in structures under seismic loads [46]. Likewise, inerter-based devices have been used in specific applications to different fields of civil engineering. Examples of this are the study of TMDI for the mitigation of wind-induced response of tall buildings [47], the use of a Tuned Damper Inerter (TID) for suppression of unwanted cable vibrations due to support excitations [48], the numerical implementation of a Tuned Parallel Inerter Mass System (TPIMS) for seismic mitigation of a wind turbine tower [49], the optimal design based on analytical solution for a liquid storage tank with a inerter isolation system [50], the optimal design and seismic performance of a TMDI when installed below the isolation floor of base-isolated structures in order to enhance the earthquake resilience and reduce the displacement demand [51], the development of a comfort-based optimal method for designing floors using Tuned Inerter Mass Systems (TIMS) to reduce the vertical-vibration response of floors subjected to human-induced excitations [52], the study of a Tuned Inerter Liquid System (TILS) for vibration control by utilizing the advantages of the inerter-based system and tuned liquid element to improve control performance [53], and the investigation of the effect of connecting TMDIs between nonconsecutive floors [54], among others.

Regarding the quoted paper by Giaralis and Petrini [54], it is suggested that an enhanced behavior is found when connecting the TMDI device located at the top floor with a floor up to three levels below, although reasonable, was considered not applicable to the work described herein, as a retrofit application is exemplified in this paper.

The main objective of the study presented here is to obtain an optimal TMDI design through an exhaustive search process, which consists in the determination of the damper critical damping ratio, ζ_{TMDI}, and frequency ratio, υ_{TMDI}, which result in the minimum structural response of a multidegree of freedom structural system, considering predefined values for mass ratio (μ) and inertance ratio (β). The proposed optimization process examines all possible damping device design parameter combinations, to select the set of values that results in the best device performance to reduce response parameters in a structure. Four different optimization processes are performed by independently minimizing four performance indices: J_1 is associated to the reduction of the structure's maximum peak displacement, J_2 calculates the minimal RMS value for the structure's peak displacement, J_3 seeks by the minimal peak interstorey drift, and J_P determines the lowest value for a linear weighted combination of the abovementioned three indices. A numerical example is developed with the purpose to validate the proposed optimization procedure and to evaluate the benefits of using TMDI as controlling devices for structures under seismic excitation, by carrying out a comparative analysis to contrast the performance of the optimization alternatives developed, running up to 1968192 cases.

This research represents a thorough and rigorous, albeit simple, optimization process applied on a model with multiple degrees of freedom. The exhaustive search-based optimization technique works efficiently in limited size problems, such as the one at hand. Furthermore, exhaustive search is reliable, easy to implement, and represents a certainty, as all possible solutions are investigated.

2. Tuned Mass Damper Inerter (TMDI)

The inerter device (Figure 1) is conceptually developed based on analogies between existing mechanical and electrical systems, as a true mechanical equivalent of the electric condenser [55].

This mechanism, characterized by a small mass in comparison with the storey mass, is an element connected to two nodes. These nodes move, respectively, from each other, generating relative accelerations that are proportional to the resisting forces produced by the device, as described by equation (1), where F is the resisting force in each node, b is the proportionality constant in terms of mass which defines the inerter, and $\ddot{u}_i$ and $\ddot{u}_j$ are the i and j nodal accelerations, respectively:

$$F = b\left(\ddot{u}_i - \ddot{u}_j\right). \tag{1}$$

Most proposed inerters are devices based on mechanisms developed from gears, racks, pinions, and flywheels

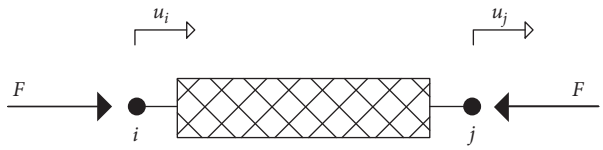

Figure 1: Outline of an inerter device.

[38, 39, 45, 56], although there are also inerter proposals based on pendulum systems [43], on ball screws [56], and on hydraulic devices [57–59].

2.1. Equation of Motion for an n Degree of Freedom System Equipped with a TMDI. To pose the equations of motion that govern an n degree of freedom system equipped with a TMDI, consider the structure shown in Figure 2. Each storey stiffness, damping, and mass is represented with a spring with stiffness constant k_i, viscous damper with damping constant c_i, and mass concentration elements m_i, respectively, where i symbolizes each level of the structure.

Likewise, the TMDI device is idealized in this figure as the combination of a conventional TMD and an inerter. In this case, the conventional TMD is installed in the n^{th} level of the building; the inerter connects the conventional TMD with the structure's level $n-1$. The TMDI mass is denoted by m_{TMDI}, while the stiffness and damping parameters associated with the damper are denoted as k_{TMDI} and c_{TMDI}, respectively. Constant b is the parameter quantifying the TMDI inertance.

In this way, the dynamic behavior of the n+1 degrees of freedom TMDI equipped system subjected to a ground acceleration at its base may be modelled with equation (2), where $\mathbf{x}(t)$, $\dot{\mathbf{x}}(t)$, and $\ddot{\mathbf{x}}(t)$ are the $n+1$ displacement, velocity, and acceleration system vectors, respectively, which depend on the variation of time, $\mathbf{1}$ is a unitary vector of the order $n+1$, and $\ddot{x}_g(t)$ is an scalar representing the ground acceleration which also varies with time.

$$\mathbf{M}\ddot{\mathbf{x}}(t) + \mathbf{C}\dot{\mathbf{x}}(t) + \mathbf{K}\mathbf{x}(t) = -\mathbf{M}\mathbf{1}\ddot{x}_g(t). \tag{2}$$

$\mathbf{M}$ is the system's mass matrix of the order $(n+1)\ x\ (n+1)$, shown with the following expression:

$$\mathbf{M} = \begin{bmatrix} m_1 & 0 & 0 & 0 & \cdots & \cdots & 0 \\ 0 & m_2 & 0 & 0 & \cdots & \cdots & 0 \\ 0 & 0 & m_3 & 0 & \cdots & \cdots & 0 \\ \vdots & \vdots & \vdots & \ddots & \cdots & \cdots & \vdots \\ \vdots & \vdots & \vdots & \vdots & m_{n-1}+b & 0 & -b \\ \vdots & \vdots & \vdots & \vdots & 0 & m_n & 0 \\ 0 & 0 & \cdots & \cdots & -b & 0 & m_{\text{TMDI}}+b \end{bmatrix}. \tag{3}$$

$\mathbf{C}$ refers to the system's damping matrix, of the order of $(n+1)\ x\ (n+1)$, expressed as

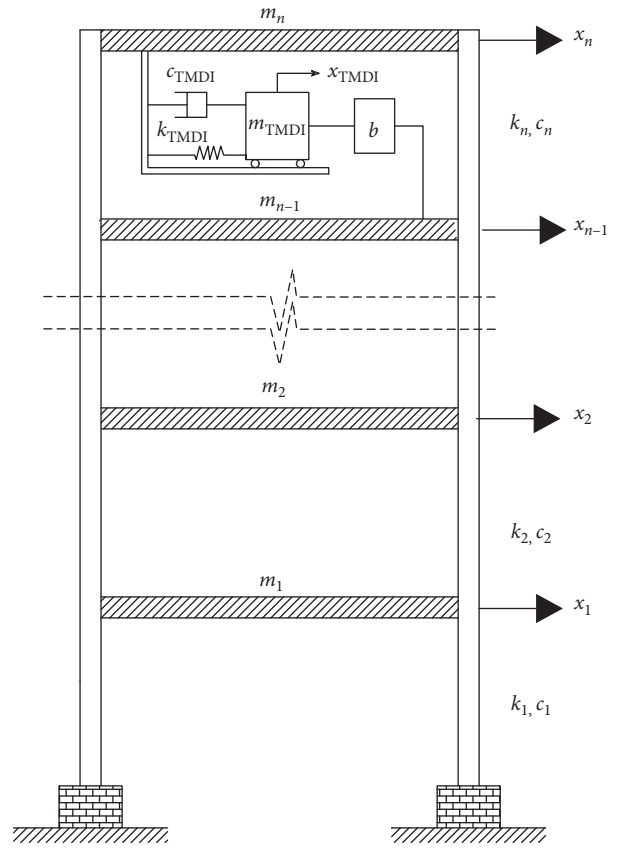

Figure 2: n degrees of freedom system equipped with a TMDI device.

$$\mathbf{C} = \begin{bmatrix} c_1+c_2 & -c_2 & 0 & 0 & \cdots & \cdots & 0 \\ -c_2 & c_2+c_3 & -c_3 & 0 & \cdots & \cdots & 0 \\ 0 & -c_3 & c_3+c_4 & -c_4 & \cdots & \cdots & 0 \\ \vdots & \vdots & \vdots & \ddots & \cdots & \cdots & \vdots \\ \vdots & \vdots & \vdots & -c_{n-1} & c_{n-1}+c_n & -c_n & 0 \\ \vdots & \vdots & \vdots & 0 & -c_n & c_n+c_{\text{TMDI}} & -c_{\text{TMDI}} \\ 0 & 0 & \cdots & 0 & 0 & -c_{\text{TMDI}} & c_{\text{TMDI}} \end{bmatrix}. \tag{4}$$

Finally, the system's stiffness matrix $\mathbf{K}$, of the order $(n+1)\ x\ (n+1)$, may be calculated as

$$\mathbf{K} = \begin{bmatrix} k_1+k_2 & -k_2 & 0 & 0 & \cdots & \cdots & 0 \\ -k_2 & k_2+k_3 & -k_3 & 0 & \cdots & \cdots & 0 \\ 0 & -k_3 & k_3+k_4 & -k_4 & \cdots & \cdots & 0 \\ \vdots & \vdots & \vdots & \ddots & \cdots & \cdots & \vdots \\ \vdots & \vdots & \vdots & -k_{n-1} & k_{n-1}+k_n & -k_n & 0 \\ \vdots & \vdots & \vdots & 0 & -k_n & k_n+k_{\text{TMDI}} & -k_{\text{TMDI}} \\ 0 & 0 & \cdots & 0 & 0 & -k_{\text{TMDI}} & k_{\text{TMDI}} \end{bmatrix}. \tag{5}$$

The motion described with equation (2) may be transformed into a space-state representation in order to more readily solve the dynamic system through first-degree differential equations. Consequently, in order to represent the n

degree of freedom system's dynamic behavior as a space-state form, the state vector $\mathbf{z}(t)$ is defined as

$$\mathbf{z}(t) = \begin{Bmatrix} \mathbf{x}(t) \\ \dot{\mathbf{x}}(t) \end{Bmatrix}, \tag{6}$$

where $\mathbf{z}(t)$ is a vector of the order $2(n+1)\ x\ 1$ containing the displacements and velocities from the structural system response. Thus, equation (2) may be transformed into equation (7), where $\mathbf{0}$ and $\mathbf{I}$ are the null and the identity matrices, respectively, of the order $(n+1)\ x\ (n+1)$.

$$\begin{Bmatrix} \dot{\mathbf{x}}(t) \\ \ddot{\mathbf{x}}(t) \end{Bmatrix} = \begin{bmatrix} \mathbf{0} & \mathbf{I} \\ -\mathbf{M}^{-1}\mathbf{K} & -\mathbf{M}^{-1}\mathbf{C} \end{bmatrix} \begin{bmatrix} \mathbf{x}(t) \\ \dot{\mathbf{x}}(t) \end{bmatrix} + \begin{bmatrix} \mathbf{0} \\ \mathbf{M}^{-1} \end{bmatrix} \cdot -\mathbf{M}1\ddot{x}_g\ (t). \tag{7}$$

Now, in order to simplify equation (7), the matrices $\mathbf{A}$ and $\mathbf{B}$ are introduced as per equations (8) and (9), where $\mathbf{A}$ is the transition state matrix, of the order $2(n+1)\ x\ 2(n+1)$, and $\mathbf{B}$ is the structural system's external excitation action location matrix:

$$\mathbf{A} = \begin{bmatrix} \mathbf{0} & \mathbf{I} \\ -\mathbf{M}^{-1}\mathbf{K} & -\mathbf{M}^{-1}\mathbf{C} \end{bmatrix}, \tag{8}$$

$$\mathbf{B} = \begin{bmatrix} \mathbf{0} \\ \mathbf{M}^{-1} \end{bmatrix}. \tag{9}$$

Thus, equation (7) becomes

$$\dot{\mathbf{z}}(t) = \mathbf{A}z(t) - \mathbf{BM1}\ddot{x}_g\ (t). \tag{10}$$

The solution for this differential linear equation of the first-degree gives the dynamic behavior of the structure equipped with the TMDI device, when subjected to an acceleration record at its base.

3. TMDI Design Optimal Parameters Selection Methodology

The optimal parameters for the design of the TMDI device are determined in this work through an optimization process based on the so-called exhaustive search technique. This optimization methodology is a general optimal parameter search technique that does not require specific knowledge of the dominion, as only a general state description, an operator set adjusted to the system's typical behavior, an initial state, and a goal or objective for the final state are needed [60].

The exhaustive search-based optimization methodologies work simply and directly, resulting in adequate and precise solutions, but require an important amount of processing time and power. Allowing for this, an exhaustive search algorithm examines all possible solutions of each particular state, continually comparing which of these possible solutions is most efficient in complying with the problem's restrictions with the lowest cost, which is usually defined with the system's own characteristics and the imposed conditions by the problem at hand.

The main motivation for the use in this paper of the exhaustive search based optimization technique is that, in limited size problems, such as the one at hand, for the selection of TMDI device parameters, the used methodology works efficiently. This must be added to the fact that exhaustive search is reliable and easy to implement when it is compared with others optimization techniques such as evolutionary algorithms, gradient-based optimization algorithms, and nature-inspired metaheuristics; furthermore, trying all possible solutions, determining an optimal state through the comparison between different final states of the problem under study, is a certainty.

TMDI devices design, using the described parameter selection procedure, consists in determining the values for the damper critical damping ratio, ζ_{TMDI}, and frequency ratio, υ_{TMDI}, which are defined according to equations (11) and (12), respectively, where c_{TMDI}, m_{TMDI} and ω_{TMDI} are the damping, mass and frequency TMDI device parameters, respectively, b is the inertance, and ω_1 is the structural system's natural fundamental frequency:

$$\zeta_{\mathrm{TMDI}} = \frac{c_{\mathrm{TMDI}}}{2\left(m_{\mathrm{TMDI}} + b\right)\omega_{\mathrm{TMDI}}}, \tag{11}$$

$$\upsilon_{\mathrm{TMDI}} = \frac{\omega_{\mathrm{TMDI}}}{\omega_1}. \tag{12}$$

The methodology starts with closed continuous sets of possible optimal values for parameters ζ_{TMDI} and υ_{TMDI}. To begin with, the process generates a division of these sets into a finite number of values, comprising the complete set of optimal values for each parameter. The optimization method uses all possible combinations of finite values generated in the process of division of the closed sets, so each one of these discrete values and its respective combination are used to calculate the TMDI damper coefficients of mass (m_{TMDI}), damping (c_{TMDI}), and stiffness (k_{TMDI}), from the mathematical manipulation of expressions (11) and (12), assuming a device mass ratio (μ) and an inertance ratio (β) whose values are constant through the whole optimization process, where μ and β are defined according to expressions (13) and (14) and m_{TMDI} and m_1 are the TMDI device mass and the generalized system mass that allows to obtain the structural system natural fundamental frequency, respectively:

$$\mu = \frac{m_{\mathrm{TMDI}}}{m_1}, \tag{13}$$

$$\beta = \frac{b}{m_1}. \tag{14}$$

Once the TMDI parameters are determined, the optimization procedure calculates the controlled structural system response when subjected to a specific acceleration record. This response is stored within a database where it is processed to determine the performance parameters that allowed establishing comparison criteria between the diverse examined device cases. After this step, the optimization process selects a new discrete value for ζ_{TMDI} and υ_{TMDI} and repeats the process anew until it obtains updated

comparison parameters according to the new used characteristics. When the exhaustive search algorithm has spent all possible solutions to the optimization problem, a comparison routine defines which are the TMDI design parameters which result in the optimized structural response, measured through the minimum values of three response parameters indices, namely, the structure's maximum peak displacement, the *RMS* value for the structure's peak displacement, and the peak storey drift:

$$\begin{aligned} J_1 &= \min\left(\max\left(\left|X_{i\text{peak}}\right|\right)\right), \\ J_2 &= \min\left(\max\left(\left|RMS\left(X_{i\text{peak}}\right)\right|\right)\right), \\ J_3 &= \min\left(\max\left(\left|\Delta_{i\text{peak}}\right|\right)\right). \end{aligned} \tag{15}$$

Furthermore, a fourth performance index is included, consisting in a linear combination of the first three indices, with specific weights, according to the relevance given to each response parameter; this linear combination is labeled as performance index, J_P, and is described with the following equation:

$$J_P = \min\left(0.5\frac{\max\left(\left|X_{i\text{peak}}\right|\right)}{J_1} + 0.3\frac{\max\left(\left|\text{RMS}\left(X_{i\text{peak}}\right)\right|\right)}{J_2} + 0.2\frac{\max\left(\left|\Delta_{i\text{peak}}\right|\right)}{J_3}\right). \tag{16}$$

These particular weights for the combination of the performance indices were defined so as to amplify the reduction of the peak displacement, although all three performance indices show reduced responses.

Figure 3 shows a logic tree diagram describing the exhaustive search algorithm parameter definition used in this study. This is the procedure used to calculate the optimal TMDI device design parameters, which controls the response of a structure subjected to seismic excitation.

4. Numerical Example for a TMDI-Equipped *n* Degree of Freedom System Optimally Designed Using the Exhaustive Search Optimization Procedure

To study the performance of a TMDI controlled system designed with the proposed exhaustive search procedure, a numerical model based on a real structure is implemented. This model is subjected to four acceleration records of natural origin, and a comparative analysis of the control device is developed.

The model used in this example is based on the building that houses Beneficencia de Antioquia, which is the governmental agency in charge of the city of Medellin's lottery, Colombia. This building has 11 levels, each with a height of 2.72 m. The structure's total height is 32.14 m above the ground level, counting the elevators' engine room and the roof. According to the Colombian earthquake resistant design code, Normas Colombianas de Diseño y Construcción Sismo Resistente, NSR-10 [61], the structure is comprised by two structural systems. In the north-south direction, parallel to the building's main facade, the structure is a reinforced concrete moment-resisting frame, while in the east-west direction, the structure is a combination of a moment-resisting frame and structural walls. Figure 4 presents an image of the modelled building; Figure 5 shows the fifth floor plan, which is a typical floor configuration, and the plane frame modelled.

The H-shaped structure was used because it is part of a larger study for seismic retrofit being conducted by the research group; however, a plane frame was derived from the original structural system; the degrees of freedom of this plane frame were reduced to one degree of freedom per storey, assuming an infinitely rigid floor diaphragm so as to obtain equal horizontal degrees of freedom for all nodes in each storey, assuming axially infinitely rigid column so as to eliminate all vertical degrees of freedom for all nodes and, finally, condensing the rotational degrees of freedom as to be expressed in terms of the remaining horizontal degrees of freedom.

Expressions (17) and (18) represent the stiffness (**K**) and mass (**M**) matrices of the reduced model, respectively. The damping matrix (**C**) is calculated as a Rayleigh damping matrix proportional to the stiffness and mass matrices, assuming a critical damping ratio of 5% for the first and last modes of vibration. Table 1 shows the modal properties of the plane frame modelled.

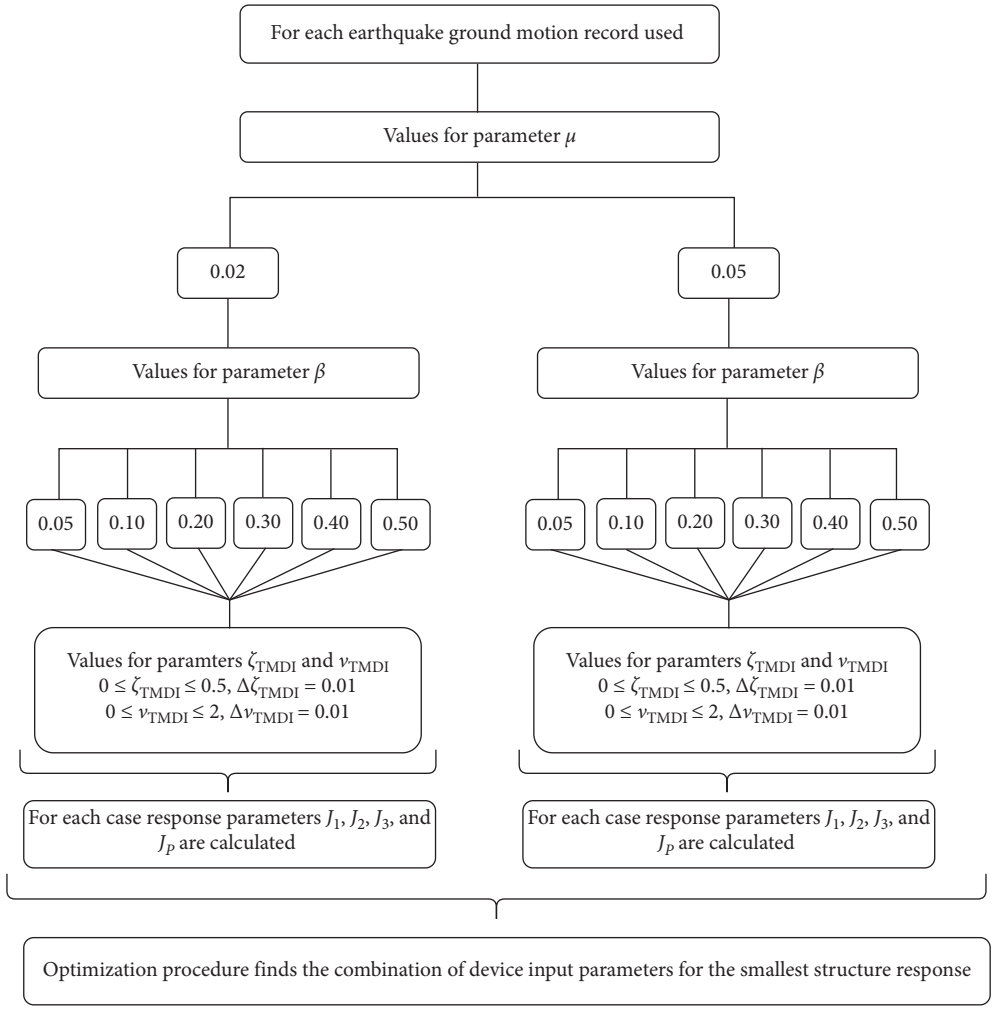

Figure 3: Logic tree diagram for TMDI device design.

Figure 4: General view of the Beneficencia de Antioquia building.

(a) (b)

Figure 5: Structure details. (a) Typical plan configuration of the modelled building. (b) Plane frame modelled.

Table 1: Modal properties of the plane frame modelled.

Mode	1	2	3	4	5	6	7	8	9	10	11
Period (s)	2.760	0.866	0.474	0.309	0.222	0.166	0.126	0.099	0.084	0.076	0.069
Natural frequency (rad/s)	2.28	7.26	13.26	20.36	28.33	37.88	49.90	63.42	75.04	82.96	91.65

$$\mathbf{K} = \begin{bmatrix} 311765 & -172446 & 48350.9 & -13110.7 & 2932 & -658.4 & 148.5 & -33.6 & 7.6 & -1.7 & 0.3 \\ & 195016 & -116165 & 44693.4 & -9953.8 & 2225.3 & -499.5 & 112.6 & -25.4 & 5.6 & -0.9 \\ & & 183933 & -148834 & 52580 & -11700.6 & 2613.6 & -586.1 & 131.7 & -28.7 & 4.6 \\ & & & 231499 & -162559 & 55631 & -12381.3 & 2765.8 & -619.2 & 134.4 & -21.4 \\ & & & & 235389 & -163428 & 55825.5 & -12424 & 2770.6 & -599.1 & 95.2 \\ & & & & & 235584 & -163470 & 55830.3 & -12403.9 & 2673 & -424.1 \\ & & & \text{SYMMETRIC} & & & 235589 & -163450 & 55732.7 & -11971.7 & 1896.5 \\ & & & & & & & 235491 & -163018 & 53819 & -8513.8 \\ & & & & & & & & 233577 & -154509 & 38358 \\ & & & & & & & & & 195586 & -85108 \\ & & & & & & & & & & 53714 \end{bmatrix} \text{kN/m}, \tag{17}$$

$$\mathbf{M} = \begin{bmatrix} 77.28 & 0 & 0 & 0 & 0 & 0 & 0 & 0 & 0 & 0 & 0 \\ & 77.94 & 0 & 0 & 0 & 0 & 0 & 0 & 0 & 0 & 0 \\ & & 78.02 & 0 & 0 & 0 & 0 & 0 & 0 & 0 & 0 \\ & & & 77.44 & 0 & 0 & 0 & 0 & 0 & 0 & 0 \\ & & & & 77.44 & 0 & 0 & 0 & 0 & 0 & 0 \\ & & & & & 77.44 & 0 & 0 & 0 & 0 & 0 \\ & & & & & & 77.44 & 0 & 0 & 0 & 0 \\ & & & \text{SYMMETRIC} & & & & 77.44 & 0 & 0 & 0 \\ & & & & & & & & 77.44 & 0 & 0 \\ & & & & & & & & & 77.44 & 0 \\ & & & & & & & & & & 74.70 \end{bmatrix} \text{Mg}. \tag{18}$$

Once the structure's model characteristics are defined, the TMDI parameter optimization procedure is initialized. This algorithm employs two fixed mass ratios, μ, of 5% and 2% and uses two close sets of optimal values for parameters ζ_{TMDI} and υ_{TMDI}, defined as

$$\begin{aligned} 0 \le \zeta_{\text{TMDI}} \le 0.5, \\ 0 \le \upsilon_{\text{TMDI}} \le 2. \end{aligned} \tag{19}$$

These value intervals have been selected because they are coherent with conventional TMD devices, serving as starting points as TMDI has the dynamic behavior same as that of conventional TMD [62].

Several inertance ratios values, β, are tried in the optimal TMDI design in order to analyze the impact of that property on the structural system response performance. With that purpose, β values of 5, 10, 20, 30, 40, and 50% were used. Both the structural model and the optimization tool were

implemented in MATLAB using routines built by the authors.

Table 2 shows the acceleration records used to excite the controlled system in order to evaluate the performance of the different TMDI configurations in the optimization process. Multiple records commonly found in the literature were used to encompass diverse acceleration inputs to show that the device works independently of the time-history demand.

4.1. Response of the Reference System (without Control). Tables 3–6 show the data obtained from the structure's response under the seismic records employed in this work for the system uncontrolled; interesting values are worth pointing out. The first one has to do with the maximum displacement magnitude, which reached 0.572 m, corresponding to the lateral movement of the building's 11th floor under the "*Kobe*" earthquake record. Secondly, the maximum displacement *RMS* corresponds also to the same floor, but under the acceleration record from "*El Centro*," which reached 0.162 m, representing 165% greater displacement *RMS* of the 11th floor under the "*Kobe*" record, which reached a value of 0.097 m. With respect to the storey drift data, the peak value was reached under the "*Kobe*" record for the horizontal relative displacement between floors 8 and 9, of 0.107 m, constituting a storey drift peak value of 3.92%. Under the "*Algarrobo*," "*El Centro*," and "*Christchurch*" records, the storey drift peak values were 0.083 m, 0.078 m, and 0.061 m, respectively, values that represent a storey drift of 3.05%, 2.86%, and 2.23%, respectively.

Only elastic analysis was considered in this study as in most codes, the principle of equivalent displacements is invoked to allow for elastic analysis for design, using a reduction factor for loads to consider the effect of plastification. The purpose of TMD and TMDI practical applications is to reduce the structural response to minimize plastification on the building frame and concentrate energy dissipation on the controlling device. In this paper, we seek to try a thorough parameter optimization process to produce reduced response; whether the final response lies inside or outside the linear behavior is out of the scope of this paper.

4.2. TMDI Optimization Process. The TMDI design parameters are obtained for four different optimization alternatives, corresponding to the evaluation of indices J_1, J_2, J_3, and J_P. To make sure the device design parameter selection corresponds to optimal parameters, a comparative analysis of the controlled structure's behavior is made for each of the TMDI parameter optimization alternatives. In this way, the comparative analysis shows the general control device performance main tendencies found with each of the optimization alternative studied.

Tables 7–10 present a summary of the parameters ζ_{TMDI} and υ_{TMDI} obtained with the optimization processes conducted for TMDI mass ratios (μ) of 2 and 5% and inertance ratios (β) of 5, 10, 20, 30, 40, and 50%. Figure 6 presents the optimal values distribution dispersion for parameters ζ_{TMDI} and υ_{TMDI} obtained through the linear combination optimization proposal (J_P), using the mass ratios and the inertance ratios values mentioned above, for the acceleration records considered.

4.3. Controlled System Response Using the Optimization Alternative JP. Table 11 presents the response parameters for the controlled structure subjected to the "*El Centro*" earthquake record for the four optimization alternatives proposed in this study. Positive and negative values in the percentage reduction columns in this table represent, respectively, a response reduction and response increase. Based on the analysis of the results data, it may be said that the TMDI controlled system performance with the greatest mass ratio ($\mu = 5\%$) is always superior to that of the lesser mass ratio ($\mu = 2\%$). The greatest peak displacement reduction of the structure, corresponding to the 11th floor displacement, is 6.76%, for the TMDI with $\mu = 2\%$ and $\beta = 5\%$ and optimizations alternatives J_P and J_1; this same parameter for the same optimizations alternatives but with device values of $\mu = 5\%$ and $\beta = 5\%$ reaches a reduction of 25.84%. Something similar occurs with the *RMS* value for the 11th floor displacement, where the greatest reduction for this parameter is obtained for the TMDI designed with values μ and β of 5%, with reductions of 46.64% for the optimization alternative J_2, while the best control alternative for TMDI designed with $\mu = 2\%$, corresponding also to the optimization alternative J_2, is that with $\beta = 5\%$, with *RMS* displacement reductions for the 11th floor of 24.47%. Finally, the peak interstorey drift reductions show that the greater the mass ratio, the greater the response parameter reduction, as the TMDI-controlled system with μ and β of 5% reduces the maximum peak storey drift in 26.22%, while the TMDI with $\mu = 2\%$ and $\beta = 5\%$ results in reductions of 12.87%.

Thus, it can be seen that the device with mass and inertance ratio values of 5% is the TMDI with the best results in terms of response parameter reduction. Likewise, the linear combination optimization alternative, J_P is, in the case of the controlled structure subjected to the "*El Centro*" earthquake, the most balanced and interesting alternative, as it results in important reductions of peak displacements and of peak storey drifts. The results clearly show that the linear combination optimization surpasses the single objective alternatives, J_2 and J_3, characteristics, generally reaching considerable reduction for all analyzed response parameters.

Figure 7 presents a graphic comparison of the 11th floor displacement evolution of the structure controlled with the TMDI configured with design parameters selected by the optimization alternative J_P for $\mu = 5\%$ and for the different values of inertance ratio used in this work. Figure 8 shows the peak storey drift ratio for each level of the building controlled by a TMDI with $\mu = 5\%$ and β between 5 and 50%.

TMDI performance optimized for the structure subjected to the "*Christchurch*" record confirms that inertance ratio (β) and mass ratio (μ) values of 5% are the parameter combination that achieves the best response reduction results when optimized using the linear combination alternative proposed in this work. For this specific load case, the peak displacement reductions are of up to 10%, while the

Table 2: Earthquake ground-motions records used in the study.

Earthquake acceleration record	Date	Earthquake location (Lat, Lon)	Magnitude
El Centro	05-18-1940	32.733°N 115.5°W	6.9 M_W
Christchurch	02-22-2011	43.583°S 172.680°E	6.2 M_W
Kobe	01-17-1995	34.59°N 135.07°E	6.9 M_W
Algarrobo	03-03-1985	33.240°S 72.040°W	8.0 M_W

Table 3: Response of the uncontrolled structure when it is excited by "*El Centro*" earthquake.

Storey	Maximum displacement (m)	*RMS* value of the displacement (cm)	Maximum velocity (m/s)	*RMS* value of the velocity (m/s)	Maximum acceleration (m/s^2)	*RMS* value of the acceleration (m/s^2)	Peak interstorey drift (m)	Peak interstorey drift ratio (%)
1	0.0280	0.010	0.1840	0.0449	6.6264	1.2309	0.028	1.03
2	0.0801	0.029	0.4587	0.1186	6.4825	1.4594	0.052	1.92
3	0.1552	0.058	0.7369	0.2011	6.8048	1.5785	0.078	2.86
4	0.2115	0.079	0.8449	0.2435	6.3304	1.5164	0.056	2.07
5	0.2583	0.098	0.9443	0.2705	5.4689	1.4371	0.062	2.27
6	0.2936	0.114	1.0937	0.2916	5.8672	1.4158	0.067	2.46
7	0.3167	0.128	1.1427	0.3107	6.8367	1.4372	0.063	2.33
8	0.3449	0.140	1.0857	0.3297	6.7817	1.3921	0.055	2.01
9	0.3812	0.150	0.8938	0.3523	5.6421	1.3339	0.047	1.73
10	0.4070	0.157	1.0476	0.3806	5.5950	1.4714	0.040	1.48
11	0.4253	0.162	1.3226	0.4096	7.5865	1.9869	0.029	1.06

Table 4: Response of the uncontrolled structure when it is excited by "*Christchurch*" earthquake.

Storey	Maximum displacement (m)	*RMS* value of the displacement (cm)	Maximum velocity (m/s)	*RMS* value of the velocity (m/s)	Maximum acceleration (m/s^2)	*RMS* value of the acceleration (m/s^2)	Peak interstorey drift (m)	Peak interstorey drift ratio (%)
1	0.0212	0.005	0.2065	0.0245	13.1273	1.2379	0.021	0.78
2	0.0589	0.014	0.3956	0.0514	10.2182	1.0456	0.039	1.42
3	0.1164	0.028	0.5804	0.0758	10.2923	0.8617	0.061	2.23
4	0.1585	0.039	0.5941	0.0976	8.3369	1.0181	0.042	1.56
5	0.1901	0.049	0.5081	0.1162	9.9784	0.9546	0.039	1.42
6	0.2181	0.058	0.5916	0.1352	9.5672	0.9775	0.036	1.34
7	0.2438	0.065	0.6688	0.1510	9.0832	0.9899	0.030	1.10
8	0.2614	0.071	0.7251	0.1625	10.3773	0.9548	0.029	1.08
9	0.2695	0.076	0.7823	0.1728	8.9451	1.0506	0.030	1.11
10	0.2735	0.079	0.7292	0.1792	9.3335	0.9107	0.023	0.84
11	0.2773	0.081	0.7733	0.1865	11.0204	1.1567	0.022	0.82

Table 5: Response of the uncontrolled structure when it is excited by "*Kobe*" earthquake.

Storey	Maximum displacement (m)	*RMS* value of the displacement (cm)	Maximum velocity (m/s)	*RMS* value of the velocity (m/s)	Maximum acceleration (m/s^2)	*RMS* value of the acceleration (m/s^2)	Peak interstorey drift (m)	Peak interstorey drift ratio (%)
1	0.0530	0.009	0.4131	0.0735	17.1382	2.2008	0.053	1.94
2	0.1455	0.026	0.9841	0.1952	18.7434	2.6221	0.093	3.40
3	0.2498	0.047	1.5908	0.3212	16.9989	2.9246	0.105	3.87
4	0.2922	0.059	1.6969	0.3614	13.4688	2.7020	0.079	2.91
5	0.3293	0.065	1.6649	0.3539	10.7163	2.2991	0.069	2.52
6	0.3674	0.068	1.7915	0.3230	11.6945	2.2243	0.090	3.31
7	0.3766	0.070	1.5227	0.2848	13.1905	2.3450	0.091	3.33
8	0.3676	0.074	1.6938	0.2550	13.4810	2.1738	0.092	3.37
9	0.4364	0.081	1.8312	0.2724	11.9120	1.8852	0.107	3.92
10	0.5145	0.090	2.0376	0.3476	12.8432	2.3581	0.098	3.61
11	0.5717	0.097	2.4486	0.4313	21.3402	3.3782	0.071	2.63

Table 6: Response of the uncontrolled structure when it is excited by "*Algarrobo*" earthquake.

Storey	Maximum displacement (m)	*RMS* value of the displacement (cm)	Maximum velocity (m/s)	*RMS* value of the velocity (m/s)	Maximum acceleration (m/s^2)	*RMS* value of the acceleration (m/s^2)	Peak interstorey drift (m)	Peak interstorey drift ratio (%)
1	0.0338	0.007	0.3153	0.0883	12.1734	3.1552	0.034	1.24
2	0.0937	0.020	0.7276	0.1926	12.6769	3.6435	0.060	2.21
3	0.1650	0.036	0.9760	0.2456	9.1539	2.9616	0.083	3.05
4	0.2128	0.045	0.9857	0.2530	11.4629	2.6324	0.048	1.77
5	0.2318	0.053	0.9905	0.2582	10.9315	2.8978	0.041	1.51
6	0.2265	0.059	0.9758	0.2614	11.2572	3.0224	0.047	1.74
7	0.2278	0.065	1.0820	0.2573	10.8552	2.8020	0.052	1.90
8	0.2303	0.069	1.0185	0.2533	9.1700	2.7801	0.063	2.30
9	0.2408	0.074	0.9051	0.2446	11.6999	2.7564	0.058	2.14
10	0.2541	0.079	0.9759	0.2533	11.2073	2.3215	0.054	1.97
11	0.2800	0.083	1.2966	0.3220	14.6872	3.9215	0.038	1.41

Table 7: TMDI optimization parameters for $\mu = 0.02$ and $\mu = 0.05$ for the structure subjected to the "*El Centro*" record.

	$\beta = 5\%$		$\beta = 10\%$		B = 20%		$\beta = 30\%$		$\beta = 40\%$		$\beta = 50\%$	
Optimization alternative	ζ_{TMDI}	v_{TMDI}	ζ_{TMDI}	v_{TMDI}	ζ_{TMDI}	v_{TMDI}	ζ_{TMDI}	v_{TMDI}	ζ_{TMDI}	v_{TMDI}	ζ_{TMDI}	v_{TMDI}
$\mu = 2\%$												
J_1	0	0.99	0	0.99	0	0.98	0	0.98	0	0.98	0	0.98
J_2	0.04	0.97	0.03	0.97	0.02	0.98	0.01	0.98	0.01	0.99	0.01	0.99
J_3	0.5	2	0	1.09	0.01	1.05	0	1.02	0	1.03	0	1.04
J_P	0	0.99	0.03	0.97	0.02	0.98	0.01	0.99	0	0.99	0	1
$\mu = 5\%$												
J_1	0	1	0	1	0	0.99	0	0.99	0	0.99	0	0.99
J_2	0.06	0.94	0.05	0.95	0.05	0.96	0.05	0.96	0.05	0.97	0.04	0.97
J_3	0.5	2	0.5	2	0.15	1.1	0.13	1.09	0.15	1.05	0.14	1.04
J_P	0	1	0	1	0.05	0.96	0.05	0.97	0.04	0.97	0.04	0.98

Table 8: TMDI optimization parameters for $\mu = 0.02$ and $\mu = 0.05$ for the structure subjected to the "*Christchurch*" record.

	$\beta = 5\%$		$\beta = 10\%$		B = 20%		$\beta = 30\%$		$\beta = 40\%$		$\beta = 50\%$	
Optimization alternative	ζ_{TMDI}	v_{TMDI}	ζ_{TMDI}	v_{TMDI}	ζ_{TMDI}	v_{TMDI}	ζ_{TMDI}	v_{TMDI}	ζ_{TMDI}	v_{TMDI}	ζ_{TMDI}	v_{TMDI}
$\mu = 2\%$												
J_1	0	0.81	0	0.83	0	0.83	0	0.82	0	0.82	0	0.83
J_2	0.05	0.93	0.04	0.94	0.03	0.95	0.03	0.96	0.03	0.96	0.03	0.97
J_3	0	0.88	0.5	2	0.5	2	0.5	2	0.5	2	0.5	2
J_P	0.04	0.92	0.04	0.93	0.03	0.94	0.03	0.95	0.03	0.96	0.03	0.96
$\mu = 5\%$												
J_1	0	0.82	0	0.83	0	0.85	0	0.85	0	0.85	0	0.85
J_2	0.09	0.86	0.08	0.88	0.07	0.9	0.06	0.91	0.06	0.92	0.05	0.93
J_3	0	0.83	0	0.9	0.5	2	0.5	2	0.5	2	0.5	2
J_P	0.07	0.85	0.07	0.87	0.06	0.89	0.05	0.9	0.05	0.91	0.05	0.92

Table 9: TMDI optimization parameters for $\mu = 0.02$ and $\mu = 0.05$ for the structure subjected to the "*Kobe*" record.

	$\beta = 5\%$		$\beta = 10\%$		$\beta = 20\%$		$\beta = 30\%$		$\beta = 40\%$		$\beta = 50\%$	
Optimization alternative	ζ_{TMDI}	v_{TMDI}	ζ_{TMDI}	v_{TMDI}	ζ_{TMDI}	v_{TMDI}	ζ_{TMDI}	v_{TMDI}	ζ_{TMDI}	v_{TMDI}	ζ_{TMDI}	v_{TMDI}
$\mu = 2\%$												
J_1	0.5	2	0.5	2	0.5	2	0.5	2	0.5	2	0.5	2
J_2	0.04	0.95	0.03	0.96	0.03	0.97	0.02	0.98	0.02	0.98	0.02	0.99
J_3	0.5	2	0.43	2	0.5	2	0.5	2	0.5	2	0.5	2
J_P	0.5	2	0.5	2	0.5	2	0.5	2	0.5	2	0.5	2
$\mu = 5\%$												
J_1	0.5	2	0.5	2	0.5	2	0.5	2	0.5	2	0.5	2
J_2	0.08	0.91	0.06	0.92	0.06	0.94	0.05	0.95	0.05	0.96	0.05	0.96
J_3	0.5	2	0.5	2	0.5	2	0.5	2	0.5	2	0.5	2
J_P	0.5	2	0.5	2	0.5	2	0.5	2	0.5	2	0.5	2

Table 10: TMDI optimization parameters for $\mu = 0.02$ and $\mu = 0.05$ for the structure subjected to the "*Algarrobo*" record.

	$\beta = 5\%$		$\beta = 10\%$		$\beta = 20\%$		$\beta = 30\%$		$\beta = 40\%$		$\beta = 50\%$	
Optimization alternative	ζ_{TMDI}	υ_{TMDI}	ζ_{TMDI}	υ_{TMDI}	ζ_{TMDI}	υ_{TMDI}	ζ_{TMDI}	υ_{TMDI}	ζ_{TMDI}	υ_{TMDI}	ζ_{TMDI}	υ_{TMDI}
$\mu = 2\%$												
J_1	0	0.87	0	0.87	0	0.87	0	0.87	0	0.88	0	0.88
J_2	0	0.86	0	0.87	0	0.87	0	0.88	0	0.88	0	0.89
J_3	0	0.9	0.5	2	0.5	2	0.5	2	0.5	2	0.5	2
J_P	0	0.87	0	0.87	0	0.87	0	0.88	0	0.88	0	0.89
$\mu = 5\%$												
J_1	0.02	0.83	0	0.84	0	0.86	0	0.88	0	0.89	0	0.9
J_2	0.06	0.83	0.03	0.85	0.01	0.86	0	0.87	0	0.88	0	0.88
J_3	0.5	2	0.5	2	0	0.93	0	0.93	0	0.94	0.5	2
J_P	0.02	0.83	0	0.84	0	0.86	0	0.88	0	0.89	0	0.89

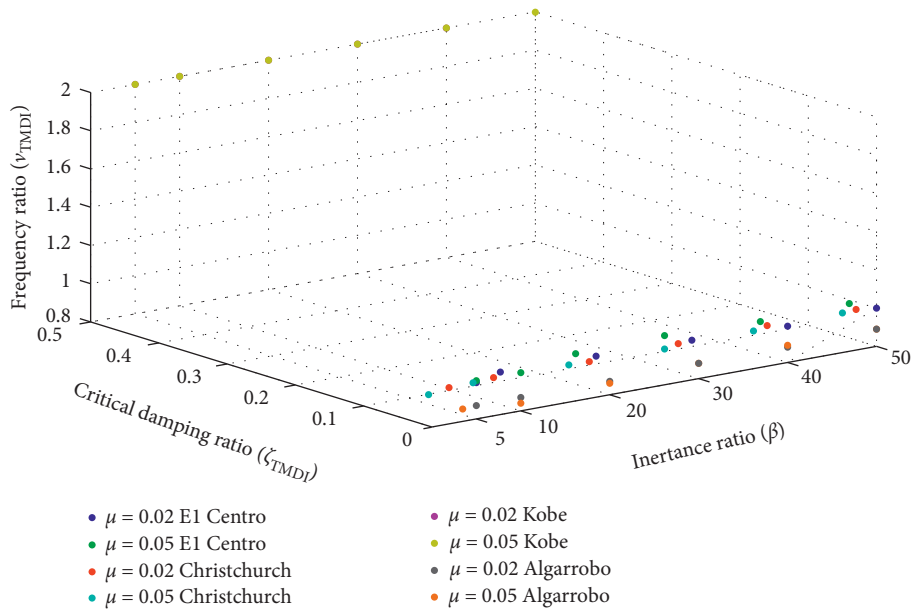

Figure 6: Distribution of the TMDI design parameters determined by the J_P optimization alternative.

Table 11: Controlled response of the structure subjected to "*El Centro*" earthquake.

β	Optimization alternative	Controlled displacement of the 11th storey (m)		Reduction of the peak displacement (%)		Controlled *RMS* value of the displacement of the 11th storey (m)		Reduction of the *RMS* value of the peak displacement (%)		Peak interstorey drift (m)		Reduction of the maximum peak interstorey drift (%)		Peak interstorey drift ratio (%)	
		$\mu = 2\%$	$\mu = 5\%$	$\mu = 2\%$	$\mu = 5\%$	$\mu = 2\%$	$\mu = 5\%$	$\mu = 2\%$	$\mu = 5\%$	$\mu = 2\%$	$\mu = 5\%$	$\mu = 2\%$	$\mu = 5\%$	$\mu = 2\%$	$\mu = 5\%$
5	J_1	0.3966	0.3154	6.76	25.84	0.1434	0.1190	11.30	26.43	0.0678	0.0574	12.87	26.22	2.49	2.11
	J_2	0.4000	0.3334	5.95	21.61	0.1221	0.0863	24.47	46.64	0.0679	0.0594	12.74	23.58	2.50	2.19
	J_3	0.4189	0.3976	1.51	6.52	0.1662	0.1651	−2.78	−2.11	0.0735	0.0620	5.53	20.34	2.70	2.28
	J_P	0.3966	0.3154	6.76	25.84	0.1434	0.1190	11.30	26.43	0.0678	0.0574	12.87	26.22	2.49	2.11
10	J_1	0.4064	0.3452	4.46	18.83	0.1415	0.1274	12.50	21.21	0.0688	0.0606	11.58	22.03	2.53	2.23
	J_2	0.4081	0.3562	4.04	16.24	0.1309	0.0975	19.04	39.73	0.0688	0.0616	11.59	20.75	2.53	2.27
	J_3	0.4081	0.4021	4.05	5.45	0.1642	0.1673	−1.53	−3.44	0.0680	0.0625	12.64	19.65	2.50	2.30
	J_P	0.4081	0.3452	4.04	18.83	0.1309	0.1274	19.04	21.21	0.0688	0.0606	11.59	22.03	2.53	2.23

Table 11: Continued.

β	Optimization alternative	Controlled displacement of the 11th storey (m)		Reduction of the peak displacement (%)		Controlled *RMS* value of the displacement of the 11th storey (m)		Reduction of the *RMS* value of the peak displacement (%)		Peak interstorey drift (m)		Reduction of the maximum peak interstorey drift (%)		Peak interstorey drift ratio (%)	
		$\mu = 2\%$	$\mu = 5\%$	$\mu = 2\%$	$\mu = 5\%$	$\mu = 2\%$	$\mu = 5\%$	$\mu = 2\%$	$\mu = 5\%$	$\mu = 2\%$	$\mu = 5\%$	$\mu = 2\%$	$\mu = 5\%$	$\mu = 2\%$	$\mu = 5\%$
20	J_1	0.4123	0.3702	3.05	12.96	0.1403	0.1396	13.24	13.70	0.0694	0.0633	10.78	18.66	2.55	2.33
	J_2	0.4132	0.3774	2.84	11.26	0.1377	0.1103	14.88	31.78	0.0692	0.0631	11.02	18.81	2.54	2.32
	J_3	0.4134	0.3904	2.80	8.21	0.1529	0.1407	5.48	12.99	0.0689	0.0602	11.48	22.65	2.53	2.21
	J_P	0.4132	0.3774	2.84	11.26	0.1377	0.1103	14.88	31.78	0.0692	0.0631	11.02	18.81	2.54	2.32
30	J_1	0.4143	0.3811	2.58	10.39	0.1415	0.1449	12.49	10.38	0.0700	0.0642	9.99	17.52	2.57	2.36
	J_2	0.4147	0.3868	2.48	9.06	0.1403	0.1172	13.22	27.52	0.0705	0.0638	9.36	18.03	2.59	2.34
	J_3	0.4145	0.3956	2.53	6.99	0.1466	0.1433	9.34	11.36	0.0693	0.0610	10.85	21.61	2.55	2.24
	J_P	0.4148	0.3867	2.48	9.07	0.1404	0.1174	13.21	27.42	0.0703	0.0636	9.66	18.24	2.58	2.34
40	J_1	0.4152	0.3872	2.37	8.95	0.1426	0.1462	11.82	9.59	0.0713	0.0646	8.35	16.95	2.62	2.37
	J_2	0.4156	0.3919	2.27	7.85	0.1415	0.1215	12.49	24.86	0.0714	0.0639	8.19	17.89	2.63	2.35
	J_3	0.4155	0.3991	2.30	6.16	0.1484	0.1420	8.20	12.21	0.0704	0.0613	9.47	21.19	2.59	2.25
	J_P	0.4152	0.3911	2.37	8.04	0.1421	0.1215	12.11	24.85	0.0710	0.0641	8.73	17.64	2.61	2.36
50	J_1	0.4156	0.3911	2.28	8.05	0.1435	0.1461	11.25	9.66	0.0722	0.0648	7.22	16.63	2.65	2.38
	J_2	0.4160	0.3945	2.18	7.25	0.1422	0.1242	12.04	23.16	0.0722	0.0642	7.21	17.48	2.65	2.36
	J_3	0.4160	0.4008	2.18	5.77	0.1500	0.1419	7.22	12.26	0.0711	0.0615	8.62	20.93	2.61	2.26
	J_P	0.4157	0.3945	2.26	7.25	0.1427	0.1244	11.78	23.08	0.0716	0.0641	7.97	17.65	2.63	2.35

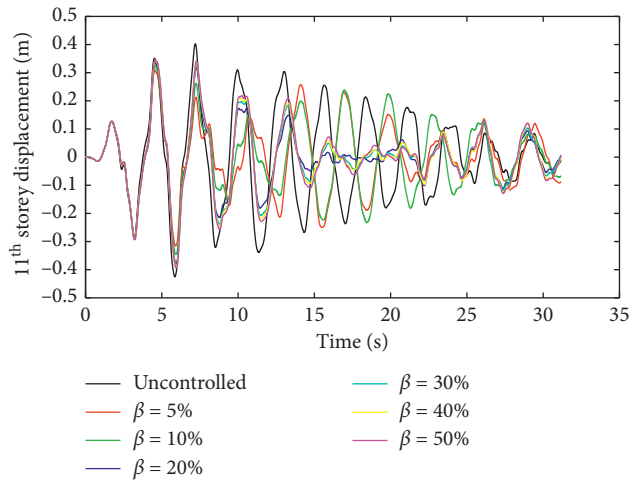

Figure 7: 11th storey controlled response of the structure subjected to "*El Centro*" acceleration record for TMDI designed with $\mu = 5\%$ and the J_P optimization alternative.

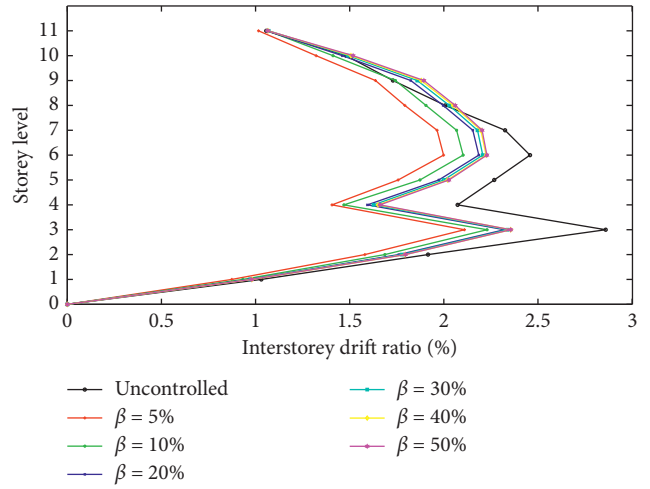

Figure 8: Interstorey drift ratio of the controlled structure subjected to "*El Centro*" acceleration record for TMDI designed with $\mu = 5\%$ and the J_P optimization alternative.

displacement *RMS* achieves up to 28% reductions. In general terms, the displacement reductions, for both the peak and the *RMS* values, present a somewhat uniform performance tendency, where small response reduction percentages are obtained for the structure's lower levels and much greater response reduction values for the last floors of the building, which is where the TMDI device exerts the greatest influence over the structural system. Figures 9 and 10 show these tendencies, for the peak displacements and the *RMS* displacements, respectively, for each one of the levels of the building, for the most efficient TMDI-controlled case, which is the one corresponding to the device with β and μ of 5% optimized with the linear combination alternative J_P.

Tables 12 and 13 present the structure's response under the "*Christchurch*" and "*Kobe*" records, respectively, for the TMDI device parameters obtained with the different optimization alternatives used in this work.

Figure 11 presents the storey peak acceleration for the controlled structure subjected to the "*Kobe*" record for the optimization alternative J_p and for a value of $\mu = 0.05$. Although all cases show important reduction for this response parameter, this time, the most efficient alternative does not correspond to the one with β of 5%, but for the optimized

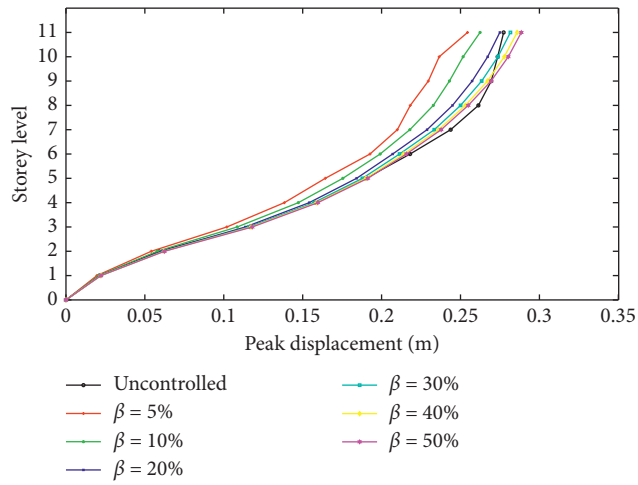

Figure 9: Peak displacement of each storey of the controlled structure subjected to "*Christchurch*" acceleration record for TMDI designed with $\mu = 5\%$ and the J_P optimization alternative.

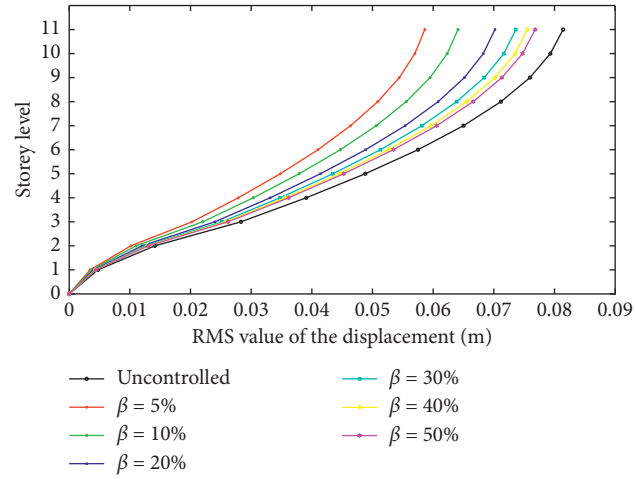

Figure 10: RMS value of the displacement of each storey of the controlled structure subjected to "*Christchurch*" acceleration record for TMDI designed with $\mu = 5\%$ and the J_P optimization alternative.

Table 12: Controlled response of the structure subjected to "*Christchurch*" earthquake.

β	Optimization alternative	Controlled displacement of the 11th storey (m)		Reduction of the peak displacement (%)		Controlled *RMS* value of the displacement of the 11th storey (m)		Reduction of the *RMS* value of the peak displacement (%)		Peak interstorey drift (m)		Reduction of the maximum peak interstorey drift (%)		Peak interstorey drift ratio (%)	
		$\mu = 2\%$	$\mu = 5\%$	$\mu = 2\%$	$\mu = 5\%$	$\mu = 2\%$	$\mu = 5\%$	$\mu = 2\%$	$\mu = 5\%$	$\mu = 2\%$	$\mu = 5\%$	$\mu = 2\%$	$\mu = 5\%$	$\mu = 2\%$	$\mu = 5\%$
5	J_1	0.2690	0.2496	3.01	10.00	0.0799	0.0798	1.87	1.93	0.0596	0.0524	1.58	13.50	2.19	1.93
	J_2	0.2740	0.2557	1.19	7.79	0.0705	0.0583	13.39	28.43	0.0598	0.0540	1.35	10.87	2.20	1.99
	J_3	0.2694	0.2496	2.86	9.98	0.0804	0.0810	1.22	0.45	0.0595	0.0523	1.87	13.72	2.19	1.92
	J_P	0.2731	0.2544	1.51	8.24	0.0706	0.0586	13.21	27.99	0.0597	0.0537	1.45	11.44	2.20	1.97
10	J_1	0.2766	0.2588	0.26	6.66	0.0819	0.0831	−0.64	−2.11	0.0608	0.0564	−0.41	6.98	2.24	2.07
	J_2	0.2801	0.2629	−1.01	5.18	0.0742	0.0640	8.81	21.37	0.0607	0.0570	−0.24	5.94	2.23	2.10
	J_3	0.2929	0.2598	−5.64	6.30	0.0887	0.0911	−8.96	−11.95	0.0588	0.0560	3.05	7.58	2.16	2.06
	J_P	0.2798	0.2624	−0.91	5.37	0.0743	0.0641	8.74	21.26	0.0607	0.0569	−0.23	6.08	2.23	2.09

Table 12: Continued.

β	Optimization alternative	Controlled displacement of the 11th storey (m)		Reduction of the peak displacement (%)		Controlled *RMS* value of the displacement of the 11th storey (m)		Reduction of the *RMS* value of the peak displacement (%)		Peak interstorey drift (m)		Reduction of the maximum peak interstorey drift (%)		Peak interstorey drift ratio (%)	
		$\mu = 2\%$	$\mu = 5\%$	$\mu = 2\%$	$\mu = 5\%$	$\mu = 2\%$	$\mu = 5\%$	$\mu = 2\%$	$\mu = 5\%$	$\mu = 2\%$	$\mu = 5\%$	$\mu = 2\%$	$\mu = 5\%$	$\mu = 2\%$	$\mu = 5\%$
20	J_1	0.2815	0.2675	−1.51	3.53	0.0836	0.0870	−2.71	−6.91	0.0616	0.0595	−1.69	1.83	2.27	2.19
	J_2	0.2840	0.2762	−2.42	0.39	0.0772	0.0701	5.21	13.92	0.0613	0.0593	−1.07	2.17	2.25	2.18
	J_3	0.2938	0.3111	−5.95	−12.18	0.0888	0.0984	−9.13	−20.86	0.0577	0.0584	4.73	3.71	2.12	2.15
	J_P	0.2838	0.2749	−2.34	0.86	0.0773	0.0702	5.09	13.77	0.0613	0.0593	−1.08	2.15	2.25	2.18
30	J_1	0.2832	0.2763	−2.14	0.38	0.0845	0.0880	−3.78	−8.13	0.0619	0.0609	−2.14	−0.46	2.28	2.24
	J_2	0.2856	0.2827	−3.00	−1.95	0.0783	0.0733	3.75	9.96	0.0613	0.0601	−1.12	0.75	2.25	2.21
	J_3	0.2945	0.3119	−6.22	−12.49	0.0889	0.0987	−9.22	−21.20	0.0572	0.0580	5.61	4.36	2.10	2.13
	J_P	0.2854	0.2816	−2.93	−1.56	0.0784	0.0736	3.73	9.55	0.0613	0.0602	−1.14	0.61	2.25	2.21
40	J_1	0.2841	0.2811	−2.45	−1.36	0.0848	0.0886	−4.20	−8.84	0.0620	0.0616	−2.29	−1.67	2.28	2.27
	J_2	0.2863	0.2868	−3.23	−3.43	0.0789	0.0753	3.06	7.44	0.0612	0.0605	−0.98	0.18	2.25	2.22
	J_3	0.2952	0.3125	−6.45	−12.71	0.0890	0.0988	−9.29	−21.41	0.0570	0.0576	6.01	4.88	2.09	2.12
	J_P	0.2863	0.2859	−3.23	−3.09	0.0789	0.0755	3.06	7.21	0.0612	0.0606	−0.98	−0.03	2.25	2.23
50	J_1	0.2845	0.2841	−2.61	−2.45	0.0848	0.0890	−4.23	−9.37	0.0620	0.0620	−2.28	−2.37	2.28	2.28
	J_2	0.2867	0.2888	−3.41	−4.16	0.0792	0.0768	2.67	5.71	0.0611	0.0607	−0.75	−0.22	2.24	2.23
	J_3	0.2957	0.3130	−6.63	−12.86	0.0890	0.0990	−9.36	−21.57	0.0569	0.0574	6.14	5.27	2.09	2.11
	J_P	0.2866	0.2885	−3.34	−4.05	0.0792	0.0768	2.64	5.63	0.0611	0.0608	−0.78	−0.27	2.25	2.23

Table 13: Controlled response of the structure subjected to "*Kobe*" earthquake.

β	Optimization alternative	Controlled displacement of the 11th storey (m)		Reduction of the peak displacement (%)		Controlled *RMS* value of the displacement of the 11th storey (m)		Reduction of the *RMS* value of the peak displacement (%)		Peak interstorey drift (m)		Reduction of the maximum peak interstorey drift (%)		Peak interstorey drift ratio (%)	
		$\mu = 2\%$	$\mu = 5\%$	$\mu = 2\%$	$\mu = 5\%$	$\mu = 2\%$	$\mu = 5\%$	$\mu = 2\%$	$\mu = 5\%$	$\mu = 2\%$	$\mu = 5\%$	$\mu = 2\%$	$\mu = 5\%$	$\mu = 2\%$	$\mu = 5\%$
5	J_1	0.5350	0.5046	6.43	11.74	0.0942	0.0931	2.38	3.50	0.0984	0.0899	7.82	15.77	3.62	3.30
	J_2	0.5590	0.5391	2.23	5.70	0.0840	0.0755	12.97	21.81	0.1071	0.1064	−0.40	0.24	3.94	3.91
	J_3	0.5350	0.5046	6.43	11.74	0.0942	0.0931	2.38	3.50	0.0984	0.0899	7.82	15.77	3.62	3.30
	J_P	0.5350	0.5046	6.43	11.74	0.0942	0.0931	2.38	3.50	0.0984	0.0899	7.82	15.77	3.62	3.30
10	J_1	0.5284	0.5015	7.57	12.27	0.0941	0.0939	2.50	2.68	0.0963	0.0893	9.72	16.29	3.54	3.28
	J_2	0.5588	0.5388	2.25	5.75	0.0862	0.0766	10.65	20.62	0.1073	0.1071	−0.53	−0.37	3.94	3.94
	J_3	0.5317	0.5015	6.99	12.27	0.0943	0.0939	2.33	2.68	0.0970	0.0893	9.13	16.29	3.56	3.28
	J_P	0.5284	0.5015	7.57	12.27	0.0941	0.0939	2.50	2.68	0.0963	0.0893	9.72	16.29	3.54	3.28
20	J_1	0.5173	0.4956	9.51	13.31	0.0936	0.0944	3.03	2.20	0.0942	0.0869	11.76	18.60	3.46	3.19
	J_2	0.5582	0.5380	2.37	5.89	0.0881	0.0791	8.70	18.07	0.1073	0.1071	−0.54	−0.36	3.94	3.94
	J_3	0.5173	0.4956	9.51	13.31	0.0936	0.0944	3.03	2.20	0.0942	0.0869	11.76	18.60	3.46	3.19
	J_P	0.5173	0.4956	9.51	13.31	0.0936	0.0944	3.03	2.20	0.0942	0.0869	11.76	18.60	3.46	3.19
30	J_1	0.5095	0.4918	10.89	13.98	0.0931	0.0944	3.50	2.13	0.0923	0.0845	13.46	20.83	3.39	3.11
	J_2	0.5580	0.5377	2.39	5.96	0.0889	0.0807	7.87	16.33	0.1078	0.1077	−0.99	−0.91	3.96	3.96
	J_3	0.5095	0.4918	10.89	13.98	0.0931	0.0944	3.50	2.13	0.0923	0.0845	13.46	20.83	3.39	3.11
	J_P	0.5095	0.4918	10.89	13.98	0.0931	0.0944	3.50	2.13	0.0923	0.0845	13.46	20.83	3.39	3.11
40	J_1	0.5045	0.4901	11.76	14.28	0.0928	0.0944	3.87	2.16	0.0907	0.0831	15.04	22.12	3.33	3.06
	J_2	0.5575	0.5370	2.49	6.08	0.0893	0.0819	7.48	15.17	0.1079	0.1082	−1.14	−1.44	3.97	3.98
	J_3	0.5045	0.4901	11.76	14.28	0.0928	0.0944	3.87	2.16	0.0907	0.0831	15.04	22.12	3.33	3.06
	J_P	0.5045	0.4901	11.76	14.28	0.0928	0.0944	3.87	2.16	0.0907	0.0831	15.04	22.12	3.33	3.06
50	J_1	0.5017	0.4899	12.24	14.30	0.0925	0.0944	4.14	2.21	0.0893	0.0824	16.31	22.75	3.28	3.03
	J_2	0.5569	0.5362	2.59	6.21	0.0894	0.0826	7.34	14.39	0.1080	0.1086	−1.19	−1.78	3.97	3.99
	J_3	0.5017	0.4899	12.24	14.30	0.0925	0.0944	4.14	2.21	0.0893	0.0824	16.31	22.75	3.28	3.03
	J_P	0.5017	0.4899	12.24	14.30	0.0925	0.0944	4.14	2.21	0.0893	0.0824	16.31	22.75	3.28	3.03

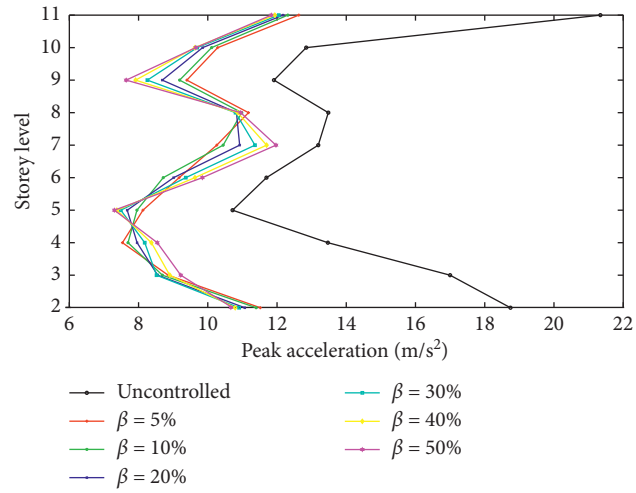

Figure 11: Peak acceleration of each storey of the controlled structure subjected to "Kobe" acceleration record for TMDI designed with $\mu = 5\%$ and the J_P optimization alternative.

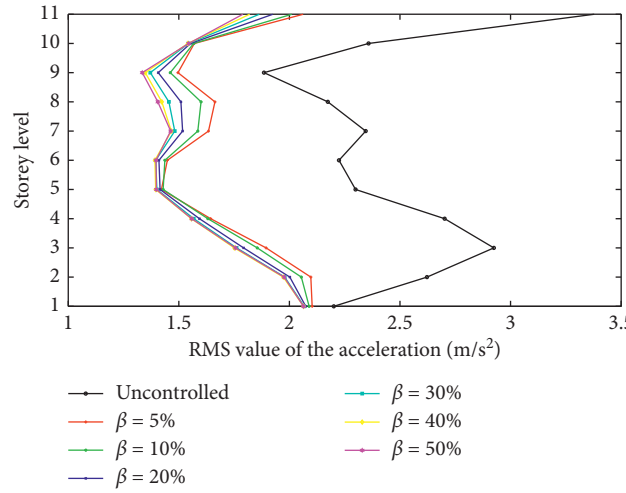

Figure 12: *RMS* value of the acceleration of each storey of the controlled structure subjected to "*Kobe*" acceleration record for TMDI designed with $\mu = 5\%$ and the J_P optimization alternative.

Table 14: Controlled response of the structure subjected to "*Algarrobo*" earthquake.

β (%)	Optimization alternative	Controlled displacement of the 11th storey (m)		Reduction of the peak displacement (%)		Controlled *RMS* value of the displacement of the 11th storey (m)		Reduction of the *RMS* value of the peak displacement (%)		Peak interstorey drift (m)		Reduction of the maximum peak interstorey drift (%)		Peak interstorey drift ratio (%)	
		$\mu = 2\%$	$\mu = 5\%$	$\mu = 2\%$	$\mu = 5\%$	$\mu = 2\%$	$\mu = 5\%$	$\mu = 2\%$	$\mu = 5\%$	$\mu = 2\%$	$\mu = 5\%$	$\mu = 2\%$	$\mu = 5\%$	$\mu = 2\%$	$\mu = 5\%$
5	J_1	0.2452	0.2251	12.45	19.59	0.0735	0.0722	11.33	12.88	0.0764	0.0722	7.96	13.07	2.81	2.65
	J_2	0.2459	0.2384	12.19	14.86	0.0732	0.0700	11.73	15.57	0.0773	0.0718	6.88	13.44	2.84	2.64
	J_3	0.2772	0.3355	0.99	−19.81	0.0812	0.0996	2.03	−20.20	0.0750	0.0764	9.69	7.90	2.76	2.81
	J_P	0.2452	0.2251	12.45	19.59	0.0735	0.0722	11.33	12.88	0.0764	0.0722	7.96	13.07	2.81	2.65
10	J_1	0.2602	0.2279	7.08	18.60	0.0752	0.0723	9.29	12.78	0.0791	0.0750	4.68	9.64	2.91	2.76
	J_2	0.2602	0.2359	7.08	15.75	0.0752	0.0705	9.29	14.94	0.0791	0.0730	4.68	12.10	2.91	2.68
	J_3	0.2957	0.3328	−5.60	−18.86	0.0861	0.0995	−3.83	−20.08	0.0775	0.0762	6.65	8.20	2.85	2.80
	J_P	0.2602	0.2279	7.08	18.60	0.0752	0.0723	9.29	12.78	0.0791	0.0750	4.68	9.64	2.91	2.76

Table 14: Continued.

β (%)	Optimization alternative	Controlled displacement of the 11th storey (m)		Reduction of the peak displacement (%)		Controlled *RMS* value of the displacement of the 11th storey (m)		Reduction of the *RMS* value of the peak displacement (%)		Peak interstorey drift (m)		Reduction of the maximum peak interstorey drift (%)		Peak interstorey drift ratio (%)	
		$\mu = 2\%$	$\mu = 5\%$	$\mu = 2\%$	$\mu = 5\%$	$\mu = 2\%$	$\mu = 5\%$	$\mu = 2\%$	$\mu = 5\%$	$\mu = 2\%$	$\mu = 5\%$	$\mu = 2\%$	$\mu = 5\%$	$\mu = 2\%$	$\mu = 5\%$
20	J_1	0.2710	0.2348	3.21	16.16	0.0773	0.0711	6.70	14.22	0.0811	0.0751	2.31	9.53	2.98	2.76
	J_2	0.2710	0.2420	3.21	13.56	0.0773	0.0711	6.70	14.23	0.0811	0.0750	2.31	9.60	2.98	2.76
	J_3	0.2923	0.3703	−4.40	−32.24	0.0859	0.0975	−3.57	−17.59	0.0754	0.0672	9.16	19.03	2.77	2.47
	J_P	0.2710	0.2348	3.21	16.16	0.0773	0.0711	6.70	14.22	0.0811	0.0751	2.31	9.53	2.98	2.76
30	J_1	0.2753	0.2404	1.68	14.16	0.0784	0.0725	5.39	12.56	0.0819	0.0743	1.37	10.52	3.01	2.73
	J_2	0.2755	0.2444	1.61	12.72	0.0783	0.0719	5.58	13.30	0.0815	0.0757	1.82	8.74	3.00	2.78
	J_3	0.2902	0.3467	−3.63	−23.80	0.0857	0.0948	−3.39	−14.38	0.0738	0.0701	11.12	15.56	2.71	2.58
	J_P	0.2755	0.2404	1.61	14.16	0.0783	0.0725	5.58	12.56	0.0815	0.0743	1.82	10.52	3.00	2.73
40	J_1	0.2775	0.2488	0.88	11.14	0.0787	0.0740	5.03	10.77	0.0819	0.0747	1.33	9.99	3.01	2.75
	J_2	0.2775	0.2509	0.88	10.41	0.0787	0.0728	5.03	12.20	0.0819	0.0760	1.33	8.45	3.01	2.79
	J_3	0.2888	0.3361	−3.14	−20.05	0.0856	0.0978	−3.26	−17.92	0.0725	0.0718	12.67	13.50	2.66	2.64
	J_P	0.2775	0.2488	0.88	11.14	0.0787	0.0740	5.03	10.77	0.0819	0.0747	1.33	9.99	3.01	2.75
50	J_1	0.2788	0.2554	0.44	8.77	0.0790	0.0757	4.68	8.69	0.0821	0.0749	1.06	9.74	3.02	2.75
	J_2	0.2792	0.2584	0.27	7.73	0.0790	0.0734	4.73	11.45	0.0818	0.0772	1.44	6.96	3.01	2.84
	J_3	0.2880	0.3254	−2.87	−16.20	0.0855	0.0993	−3.18	−19.83	0.0715	0.0722	13.91	13.06	2.63	2.65
	J_P	0.2792	0.2558	0.27	8.63	0.0790	0.0738	4.73	10.93	0.0818	0.0760	1.44	8.42	3.01	2.79

TMDI with β of 50%. In fact, for the peak storey acceleration, the linear combination optimized, J_P, TMDI with μ and β of 5% is the case with smaller reduction values of all the optimization alternatives analyzed; the same situation may be seen in Figure 12 for storey acceleration *RMS* values.

Figure 8 shows trends characteristic of drift variation with respect to height in a moment-resistant frame, with maximum drifts occurring at the third lower part of the structure's total height. Similar trends are shown in Figures 11 and 12 for floor accelerations, which are also characteristic of acceleration distribution for ultimate lateral loading, where accelerations tend to decrease with height, with respect to ground acceleration, except for the floors of the upper quarter of the structure, which tend to increase markedly. By contrast, Figures 9 and 10 show the absolute displacement distribution, which characteristically increase with height, with a higher rate of increase in the middle third of the structure's total height.

Table 14 presents the controlled structure's response values obtained for the different optimization alternatives developed, when subjected to the "*Algarrobo*" record.

For this case, the controlled system's response reduction, under the *Algarrobo* record, shows that the inerter device with mass ratio and inertance ratio of 5% achieves the best performance. Figure 13 shows the greatest peak displacement reduction for μ and β of 5%; however, as the inertance ratio, β, increases, the reduction percentage diminishes, that is, the peak displacements increase, almost linearly for a mass ratio, μ, of 5%, and asymptotically for μ of 2%

Figure 14 presents the reduction of the 11th storey *RMS* value of displacement of the structure subjected to "Algarrobo" acceleration record. For this case, results also show that the optimized device using the linear combination alternative achieves the best results for μ of 5%, but for this input seismic record, the greatest reduction is achieved in conjunction with β of 20%, although the variation of the reduction percentage for μ of 5% does not vary beyond 20% of the maximum as β varies. For TMDI designed with μ of 2%, reductions are highest for β of 5%, and reduction decreases asymptotically as β increases.

Finally, Figure 15 shows the peak storey drift reduction for the controlled structure under the "*Algarrobo*" record. For this case, results also show that the optimized device using the linear combination alternative achieves the best results for μ and β of 5%, with reductions decreasing significantly for β of 10%, and with no significant variation as β increases further. For μ of 2%, reductions are the highest for β of 5%, and reduction decreases asymptotically as β increases.

The response results shown in Figure 11 through 15 show that the TMDIs effectively reduces the structural system response for all combinations of μ and β; moreover, the graphs show that the highest reductions are obtained for peak interstorey drift with μ and β of 5%. That is, the drift is effectively reduced for all inertance ratio values, which implies a reduction of damages under seismic excitations.

5. Conclusions

This paper deals with the optimal design of TMDI using exhaustive search. The used methodology focuses on determining the best combination of parameters, so the optimal device is able to reduce the response of a structural system, through the single and combined control of three different response parameters: structure's maximum peak displacement, RMS value for the structure's peak displacement, and peak interstorey drift. The tuned mass damper inerter designed optimally have a significant potential for the response reduction of multiple degree of freedom systems under seismic excitations. The obtained results show that those devices with fixed mass ratio (μ) and

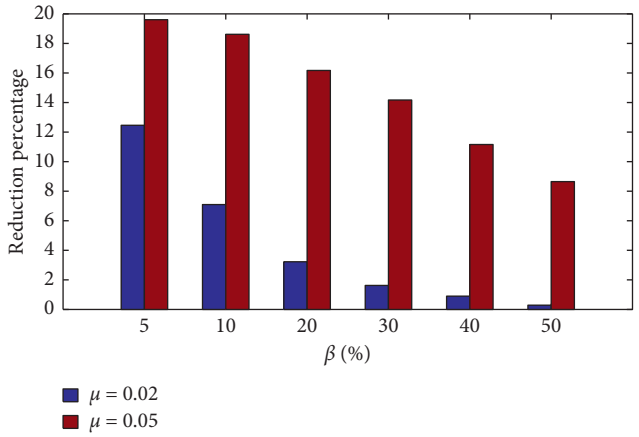

Figure 13: Comparison of the reduction of the 11th storey peak displacement of the structure subjected to "*Algarrobo*" acceleration record for TMDI designed with $\mu = 2\%$ and $\mu = 5\%$ using the J_P optimization alternative.

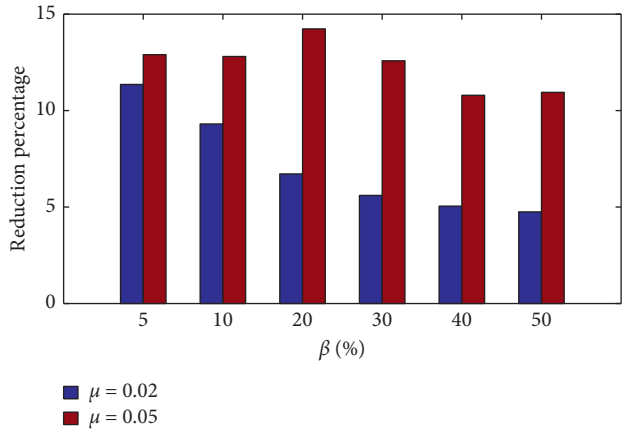

Figure 14: Comparison of the reduction of the 11th storey *RMS* value of displacement of the structure subjected to "*Algarrobo*" acceleration record for TMDI designed with $\mu = 2\%$ and $\mu = 5\%$ using the J_P optimization alternative.

inertance ratio (β) of 5% achieved the greatest last floor reductions of peak displacements and *RMS* displacement values, for mean values of critical damping ratio (ζ_{TMDI}) and frequency ratio (υ_{TMDI}), of 0.03 and 0.89, respectively, with reductions of up to 25%, for peak displacement, and up to 46% for *RMS* displacement values. For these design parameters, the maximum peak storey drift ratio reductions are of the order of 26%. Based on these results, it may be said that the linear combination optimization alternative is a valuable tool of easy implementation for the determination of optimal design parameters for TMDI devices in structural systems subjected to seismic actions. Nonlinear analysis inclusion on this topic should be the subject of future developments on this field to ensure practical applications of TMDI devices.

Data Availability

All data included in this study are available upon request by contact with the corresponding author.

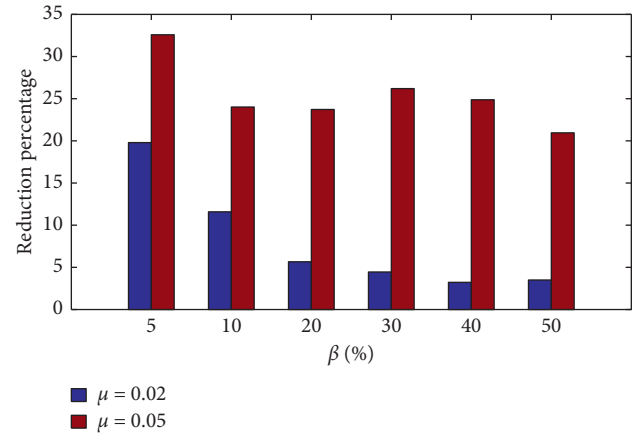

Figure 15: Comparison of the reduction of the peak interstorey drift of the structure subjected to "*Algarrobo*" acceleration record for TMDI designed with $\mu = 2\%$ and $\mu = 5\%$ using the J_P optimization alternative.

Conflicts of Interest

The authors declare that there are no conflicts of interest regarding the publication of this article.

Acknowledgments

The authors are grateful for the support provided by the Universidad Nacional de Colombia-Campus Medellin for the development of this work. Universidad Nacional de Colombia, Campus Medellin, supported the research carried out in this paper.

References

[1] G. W. Housner, L. A. Bergman, T. K. Caughey et al., "Structural control: past, present, and future," *Journal of Engineering Mechanics*, vol. 123, no. 9, pp. 897–971, 1997.

[2] S. Smanchai and J. Yao, "Active control of building structures," *Journal of the Engineering Mechanics Division*, vol. 104, no. 2, pp. 335–350, 1978.

[3] S. Pourzeynali, H. H. Lavasani, and A. H. Modarayi, "Active control of high rise building structures using fuzzy logic and genetic algorithms," *Engineering Structures*, vol. 29, no. 3, pp. 346–357, 2007.

[4] H. Khodabandolehlou, G. Pekcan, M. S. Fadali, and M. M. A. Salem, "Active neural predictive control of seismically isolated structures," *Structural Control and Health Monitoring*, vol. 25, pp. 1–15, 2018.

[5] T. T. Soong and M. C. Costantinou, *Passive and Active Structural Vibration Control in Civil Engineering*, Springer Vienna, Vienna, Australia, 1994.

[6] M. Basili and M. De Angelis, "Optimal passive control of adjacent structures interconnected with nonlinear hysteretic devices," *Journal of Sound and Vibration*, vol. 301, no. 1-2, pp. 106–125, 2007.

[7] Z. Zhang and T. Balendra, "Passive control of bilinear hysteretic structures by tuned mass damper for narrow band seismic motions," *Engineering Structures*, vol. 54, pp. 103–111, 2013.

[8] A. Arzeytoon, A. A. Golafshani, V. Toufigh, and H. Mohammadi, "Seismic performance of ribbed bracing

system in passive control of structures," *Journal of Vibration and Control*, vol. 23, no. 18, pp. 2926–2941, 2017.

[9] S. Elias, V. Matsagar, and T. K. Datta, "Distributed tuned mass dampers for multi-mode control of benchmark building under seismic excitations," *Journal of Earthquake Engineering*, vol. 23, no. 7, pp. 1137–1172, 2019.

[10] D. De Domenico, G. Ricciardi, and I. Takewaki, "Design strategies of viscous dampers for seismic protection of building structures: a review," *Soil Dynamics and Earthquake Engineering*, vol. 118, pp. 144–165, 2019.

[11] Z.-D. Xu, Y.-P. Shen, and Y.-Q. Guo, "Semi-active control of structures incorporated with magnetorheological dampers using neural networks," *Smart Materials and Structures*, vol. 12, no. 1, pp. 80–87, 2003.

[12] A. K-Karamodin and H. H-Kazemi, "Semi-active control of structures using neuro-predictive algorithm for MR dampers," *Structural Control and Health Monitoring*, vol. 17, 2008.

[13] M. Behrooz, X. Wang, and F. Gordaninejad, "Modeling of a new semi-active/passive magnetorheological elastomer isolator," *Smart Materials and Structures*, vol. 23, no. 4, p. 045013, 2014.

[14] A. Bathaei, S. M. Zahrai, and M. Ramezani, "Semi-active seismic control of an 11-DOF building model with TMD+MR damper using type-1 and -2 fuzzy algorithms," *Journal of Vibration and Control*, vol. 24, no. 13, pp. 2938–2953, 2018.

[15] R. K. Mohammadi and S. Najarzade, "Semi-active control of structures equipped with MR dampers based on uniform deformation theory," *International Journal of Civil Engineering*, vol. 16, no. 8, pp. 871–885, 2018.

[16] J. N. Yang, Z. Li, A. Danielians, and S. C. Liu, "Aseismic hybrid control of nonlinear and hysteretic structures I," *Journal of Engineering Mechanics*, vol. 118, no. 7, pp. 1423–1440, 1992.

[17] R. S. Subramaniam, A. M. Reinhorn, M. A. Riley, and S. Nagarajaiah, "Hybrid control of structures using fuzzy logic," *Computer-Aided Civil and Infrastructure Engineering*, vol. 11, no. 1, pp. 1–17, 1996.

[18] H. Kim and H. Adeli, "Hybrid control of irregular steel highrise building structures under seismic excitations," *International Journal for Numerical Methods in Engineering*, vol. 63, no. 12, pp. 1757–1774, 2005.

[19] E. Omidi and N. Mahmoodi, "Hybrid positive feedback control for active vibration attenuation of flexible structures," *IEEE/ASME Transactions on Mechatronics*, vol. 20, no. 4, pp. 1790–1797, 2015.

[20] M. Taniguchi, K. Fujita, M. Tsuji, and I. Takewaki, "Hybrid control system for greater resilience using multiple isolation and building connection," *Frontiers in Built Environment*, vol. 2, pp. 1–10, 2016.

[21] R. Rana and T. T. Soong, "Parametric study and simplified design of tuned mass dampers," *Engineering Structures*, vol. 20, no. 3, pp. 193–204, 1998.

[22] T. Pinkaew, P. Lukkunaprasit, and P. Chatupote, "Seismic effectiveness of tuned mass dampers for damage reduction of structures," *Engineering Structures*, vol. 25, no. 1, pp. 39–46, 2003.

[23] T. Engle, H. Mahmoud, and A. Chulahwat, "Hybrid tuned mass damper and isolation floor slab system optimized for vibration control," *Journal of Earthquake Engineering*, vol. 19, no. 8, pp. 1197–1221, 2015.

[24] D. De Domenico and G. Ricciardi, "Earthquake-resilient design of base isolated buildings with TMD at basement: application to a case study," *Soil Dynamics and Earthquake Engineering*, vol. 113, pp. 503–521, 2018.

[25] J. Xiang, T. Matsumoto, Y. Wang, and Z. Jiang, "A hybrid of interval wavelets and wavelet finite element model for damage detection in structures," *CMES-Computer Modeling in Engineering & Sciences*, vol. 81, pp. 269–294, 2011.

[26] P. Xiang and A. Nishitani, "Optimum design for more effective tuned mass damper system and its application to base-isolated buildings," *Structural Control and Health Monitoring*, vol. 21, no. 1, pp. 98–114, 2014.

[27] E. Matta and A. De Stefano, "Robust design of mass-uncertain rolling-pendulum TMDs for the seismic protection of buildings," *Mechanical Systems and Signal Processing*, vol. 23, no. 1, pp. 127–147, 2009.

[28] G. C. Marano and R. Greco, "Robust optimum design of tuned mass dampers for high-rise buildings under moderate earthquakes," *The Structural Design of Tall and Special Buildings*, vol. 18, no. 8, pp. 823–838, 2009.

[29] A. Lucchini, R. Greco, G. C. Marano, and G. Monti, "Robust design of tuned mass damper systems for seismic protection of multistory buildings," *Journal of Structural Engineering*, vol. 140, no. 8, 2014.

[30] R. Greco, A. Lucchini, and G. C. Marano, "Robust design of tuned mass dampers installed on multi-degree-of-freedom structures subjected to seismic action," *Engineering Optimization*, vol. 47, no. 8, pp. 1009–1030, 2015.

[31] A. Farshidianfar and S. Soheili, "Ant colony optimization of tuned mass dampers for earthquake oscillations of high-rise structures including soil-structure interaction," *Soil Dynamics and Earthquake Engineering*, vol. 51, pp. 14–22, 2013.

[32] G. Bekdaş and S. M. Nigdeli, "Metaheuristic based optimization of tuned mass dampers under earthquake excitation by considering soil-structure interaction," *Soil Dynamics and Earthquake Engineering*, vol. 92, pp. 443–461, 2017.

[33] J. Salvi, F. Pioldi, and E. Rizzi, "Optimum tuned mass dampers under seismic soil-structure interaction," *Soil Dynamics and Earthquake Engineering*, vol. 114, pp. 576–597, 2018.

[34] Y Daniel, O Lavan, and R Levy, "Multiple-tuned mass dampers for multimodal control of pedestrian bridges," *J Struct Eng*, vol. 138, pp. 1173–1178, 2012.

[35] Z. Lu, X. Chen, X. Li, and P. Li, "Optimization and application of multiple tuned mass dampers in the vibration control of pedestrian bridges," *Structural Engineering and Mechanics*, vol. 62, no. 1, pp. 55–64, 2017.

[36] M. Gutierrez Soto and H. Adeli, "Tuned mass dampers," *Archives of Computational Methods in Engineering*, vol. 20, no. 4, pp. 419–431, 2013.

[37] L. Marian and A. Giaralis, "Optimal design of a novel tuned mass-damper-inerter (TMDI) passive vibration control configuration for stochastically support-excited structural systems," *Probabilistic Engineering Mechanics*, vol. 38, pp. 156–164, 2014.

[38] P. Brzeski, T. Kapitaniak, and P. Perlikowski, "Novel type of tuned mass damper with inerter which enables changes of inertance," *Journal of Sound and Vibration*, vol. 349, pp. 56–66, 2015.

[39] P. Brzeski, M. Lazarek, and P. Perlikowski, "Experimental study of the novel tuned mass damper with inerter which enables changes of inertance," *Journal of Sound and Vibration*, vol. 404, pp. 47–57, 2017.

[40] Y. Wen, Z. Chen, and X. Hua, "Design and evaluation of tuned inerter-based dampers for the seismic control of MDOF structures," *Journal of Structural Engineering*, vol. 143, no. 4, pp. 1–11, 2017.

[41] D. De Domenico and G. Ricciardi, "An enhanced base isolation system equipped with optimal tuned mass damper inerter (TMDI)," *Earthquake Engineering & Structural Dynamics*, vol. 47, no. 5, pp. 1169–1192, 2018.

[42] D. De Domenico, H. Qiao, Q. Wang et al., "Optimal design and seismic performance of multi-tuned mass damper inerter (MTMDI) applied to adjacent high-rise buildings," *The Structural Design of Tall and Special Buildings*, Article ID e1781, 2020.

[43] P. Brzeski, E. Pavlovskaia, T. Kapitaniak, and P. Perlikowski, "The application of inerter in tuned mass absorber," *International Journal of Non-linear Mechanics*, vol. 70, pp. 20–29, 2015.

[44] D. Pietrosanti, M. De Angelis, and M. Basili, "Optimal design and performance evaluation of systems with tuned mass damper inerter (TMDI)," *Earthquake Engineering & Structural Dynamics*, vol. 46, no. 8, pp. 1367–1388, 2017.

[45] L. Marian and A. Giaralis, "The tuned mass–damper-inerter for harmonic vibrations suppression, attached mass reduction, and energy harvesting," *Smart Structures and Systems*, vol. 19, no. 6, pp. 665–678, 2017.

[46] A. Giaralis and A. A. Taflanidis, "Optimal tuned mass-damper-inerter (TMDI) design for seismically excited MDOF structures with model uncertainties based on reliability criteria," *Structural Control and Health Monitoring*, vol. 25, no. 2, pp. 1–22, 2018.

[47] Q. Wang, H. Qiao, D. De Domenico et al., "Wind-induced response control of high-rise buildings using inerter-based vibration absorbers," *Applied Sciences*, vol. 9, no. 23, p. 5045, 2019.

[48] I. F. Lazar, S. A. Neild, and D. J. Wagg, "Vibration suppression of cables using tuned inerter dampers," *Engineering Structures*, vol. 122, pp. 62–71, 2016.

[49] R. Zhang, Z. Zhao, and K. Dai, "Seismic response mitigation of a wind turbine tower using a tuned parallel inerter mass system," *Engineering Structures*, vol. 180, pp. 29–39, 2019.

[50] Y. Jiang, Z. Zhao, R. Zhang, D. De Domenico, and C. Pan, "Optimal design based on analytical solution for storage tank with inerter isolation system," *Soil Dynamics and Earthquake Engineering*, vol. 129, Article ID 105924, 2020.

[51] D. De Domenico and G. Ricciardi, "Optimal design and seismic performance of tuned mass damper inerter (TMDI) for structures with nonlinear base isolation systems," *Earthquake Engineering & Structural Dynamics*, vol. 47, pp. 2539–2560, 2018.

[52] Q. Chen, Z. Zhao, Y. Xia, C. Pan, H. Luo, and R. Zhang, "Comfort based floor design employing tuned inerter mass system," *Journal of Sound and Vibration*, vol. 458, pp. 143–157, 2019.

[53] Z. Zhao, R. Zhang, Y. Jiang, and C. Pan, "A tuned liquid inerter system for vibration control," *International Journal of Mechanical Sciences*, vol. 164, Article ID 105171, 2019.

[54] A. Giaralis and F. Petrini, "Wind-induced vibration mitigation in tall buildings using the tuned mass-damper-inerter," *Journal of Structural Engineering*, vol. 143, no. 9, Article ID 04017127, 2017.

[55] M. C. Smith, "Synthesis of mechanical networks: the inerter," *IEEE Transactions on Automatic Control*, vol. 47, no. 10, pp. 1648–1662, 2002.

[56] C. Papageorgiou and M. C. Smith, "Laboratory experimental testing of inerters," in *Proceedings of the 44th IEEE Conference on Decision and Control*, IEEE, Seville, Spain, pp. 3351–3356, 2005.

[57] F.-C. Wang, M.-F. Hong, and T.-C. Lin, "Designing and testing a hydraulic inerter," *Proceedings of the Institution of Mechanical Engineers, Part C: Journal of Mechanical Engineering Science*, vol. 225, no. 1, pp. 66–72, 2011.

[58] S. J. Swift, M. C. Smith, A. R. Glover, C. Papageorgiou, B. Gartner, and N. E. Houghton, "Design and modelling of a fluid inerter," *International Journal of Control*, vol. 86, no. 11, pp. 2035–2051, 2013.

[59] D. De Domenico, P. Deastra, G. Ricciardi, N. D. Sims, and D. J. Wagg, "Novel fluid inerter based tuned mass dampers for optimised structural control of base-isolated buildings," *Journal of the Franklin Institute*, vol. 356, no. 14, pp. 7626–7649, 2019.

[60] R. E. Korf, "Artificial intelligence search algorithms," in *Handbook of Algorithms and Theory of Computation (Chapter 36)*, CRC Press, Boca Raton, FL, USA, 1996.

[61] Ministerio de Ambiente Vivienda y Desarrollo Territorial, *Reglamento Colombiano de Construcción Sismo Resistente "NSR-10" Bogota*, Asociación Colombiana de Ingeniería Sísmica, Bogota, Colombia, 2010.

[62] L. Marian, "The tuned mass damper inerter for passive vibration control and energy harvesting in dynamically excited structural systems," Doctoral Dissertation, City University London, London, UK, 2015.